’09 춘계학술대회 우수 논문

Ag 필름/ Cu기판의 나노인덴테이션 거동 해석

트란 딘 롱*, 김엄기*, 전성식*+

Nanoindentation behaviours of silver film/copper substrate

Long Trandinh*, Amkee Kim* and Seong Sik Cheon*+

ABSTRACT

Nanoindentation behaviours on the films of softer Ag film/harder Cu substrate structure were studied by the molecular dynamics method. As a result, it was shown that the stiffness and hardness of films were strongly dependent on the thickness of films. The stiffness and hardness increased with the thickness of film within a critical range as an inverse Hall-Petch relation. The stiffness and hardness of Cu substrate with Ag film less than 5 nm were observed to be lower than those of bulk silver. In particular, the flower-like dislocation loop was created on the interface by the interaction between dislocation pile-up and misfit dislocation during the indentation of Ag film/Cu substrate with film thickness less than 4 nm, which seemed to be associated with the drop of load in the indentation load versus displacement curve.

초 록

본 논문에서는 분자동력학 방법을 이용하여 Ag 필름/Cu기판에 대한 나노인덴테이션 특성을 파악하였다. 필름의 강성과 경도는 필름의 두께에 관계되어있으며, 임계범위 내에서, 그래인 크기가 증가하면 강성과 경도도증가하는 것을 확인하였다. 5 nm 두께 이하의Ag필름/Cu기판의 강성과 경도는 벌크 Ag의 경우에 비해 낮은 값을 나타내었다. 특히 4nm 두께 이하의 Ag필름/Cu기판의 인덴테이션에 있어서, 전위 집적과 불일치 전위사이의 상호작용에 의해 계면상에서 꽃모양의 전위 루프가 발생하였다. 이는 인덴테이션 하중과 변위 커브에서 하중이 저하되는 것과 관계있는 것으로 사료되고 있다.

Key Words : 나노인덴테이션(nanoindentation), 불일치전위(misfit dislocation), 적층결함(stacking faults), 집적(pile-up)

1. Introduction

Mechanical deformation, fracture, and friction of solids and thin films propose some of the most interesting computational challenges for atomistic calculations of materials properties. The fundamental goal is to establish a connection between atomic scale processes and measurable mechanical properties of materials. Recently, the indentations of geometrically confined nanostructures such as multilayered thin films are attracting attention because the nanoindentation technique could provide the curve of the load on the indenter tip versus the tip displacement for the analysis of the mechanical properties (e.g. elastic modulus, yield stress and hardness) at a small scale.

The effect of the interface of oriented Ag/Cu bi-crystalline structure on the material transport along the interface has been studied in the temperature range of 593-882 K [1] based on radiotracer experiment. It revealed that the anisotropic misfit dislocation arrays formed at the interphase boundary (011) due to the diffusion of atoms. The molecular

* 국립공주대학교 공과대학 기계자동차공학부
*+ 국립공주대학교 공과대학 기계자동차공학부, 교신저자(E-mail:sscheon@kongju.ac.kr)

dynamics (MD) simulation also demonstrated that the misfit dislocations could be displaced out of the interface plane influencing the elastic modulus of materials [2]. Moreover, the misfit dislocation at interfaces could be one of main controlling parameters for plasticity in multilayer metals [3-5].

The mechanical properties of the softer Ag film/ harder Cu substrate bi-layer structure would be expected to be influenced by the misfit dislocation at phase interfaces. In particular, the stiffness and hardness of Ag film/ harder Cu substrate are important since they may provide the essential knowledge for the design of nano-electromechanical systems (NEMS).

In this study, the nanoindentation behaviours [6, 7] on the thin films of Ag film/Cu are simulated by MD method. The mechanism for the movement of misfit dislocation at the interface, the shape of dislocation clusters and the energy transformation of dislocations are investigated during the indentation. The thickness effect on the hardness of film in Ag film/Cu substrate and Cu film/Ag substrate is discussed based on the mechanism for the movement of misfit dislocation at the interface and the inverse Hall-Petch relation.

2. Simulation details

Nanoindentation simulations on Ag film/Cu substrate were carried out by MD method. Cu substrate with the thickness of 7 nm was chosen for the models while the thickness of Ag film was various in a range from 2 nm to 5 nm. Crystalline directions of silver and copper were (100), lattice constant a_1 = 0.409 nm and a_2 = 0.361 nm were used for silver and copper, respectively. The transverse dimensions for all models of 12 nm × 12 nm were chosen to suit to crystalline directions and lattice constants of the two metals. Although the actual distance between silver and copper atom layers at the interface in the model would be in the interval of $a_1/2$ and $a_2/2$ for the face-centred cubic (fcc) structure depending on the pair potential of two different type atoms, the average of halves of the lattice constants $(a_1/2+a_2/2)/2$ was used as an initial distance in this study because the actual distance can be achieved by the energy equilibrium through the MD relaxation process. Some bottom atom layer was fixed while periodic boundary condition was applied for side surfaces of model. Moreover, because of lattice constant mismatch of the two metals and the periodic boundary condition for side surface, the transverse dimensions of model had to be carefully calculated for minimising initial strain. Therefore, the transverse length of model was determined as follows:

$$l = \beta_1 a_1 n_1 = \beta_2 a_2 n_2 \tag{1}$$

Where a_1 and a_2 are lattice constants of two metals, n_1 and n_2 are the numbers of periodicity-length, β_1 and β_2 are periodic coefficients. The value of β depends on the direction of crystal, some values of β are expressed in Table 1. In case of Ag film/ Cu substrate model, both crystalline directions of (100), the periodic coefficients would be equal to one (β_1 = β_2 = 1), and the transverse dimensions were achieved by determining the minimum tolerance of the coefficient $\varepsilon = n_1/n_2 - a_2/a_1$. It was equivalent to n_1 = 30 periodicity-length for silver and n_2 = 34 periodicity-length for copper. The subtraction of the periodicity-lengths ($k = n_2 - n_1$) is the number of misfit space. As a result, the size is approximately 12 nm for the both transverse directions.

Table 1 Values of for face-centered cubic structure

Directions	β	Directions	β
⟨100⟩	1	⟨117⟩	$\sqrt{51}$
⟨110⟩	$\sqrt{2}/2$	⟨118⟩	$\sqrt{66}/2$
⟨111⟩	$\sqrt{3}$	⟨221⟩	$\sqrt{9}$
⟨112⟩	$\sqrt{6}/2$	⟨332⟩	$\sqrt{22}/2$
⟨113⟩	$\sqrt{11}$	⟨552⟩	$\sqrt{54}/2$
⟨114⟩	$\sqrt{18}/2$	⟨554⟩	$\sqrt{6}/2$
⟨115⟩	$\sqrt{27}$	⟨771⟩	$\sqrt{99}$

Embedded Atom Method (EAM) [8] was employed for the simulation using potential functions curve fitted by Wadley at al. [9] for the copper and silver. Simultaneously, the Johnson's formula [10] was implemented for the pair potential between copper and silver atoms as following

$$\phi^{ab}(r) = \frac{1}{2}\left(\frac{f^b(r)}{f^a(r)}\phi^{aa}(r) + \frac{f^a(r)}{f^b(r)}\phi^{bb}(r)\right) \tag{2}$$

Where *a, b* indicate atom type, $f(r)$ is electric density function and $\phi(r)$ is a pair potential function. All simulations of indentation were carried out by parallel molecular dynamics program LAMMPS [11] with radius of a spherical indenter of 4.0nm. Prior to indenting on surface, the models were relaxed by the energy minimization based on the

conjugate gradient method for the simulations at zero temperature while Nose-Hoover dynamic relaxation was used for the simulations at room temperature (300K) for 30 ps. In order to compare indentation behaviours of Ag film/copper substrate to those of bulk copper and bulk silver, the indentations on bulk copper (100) and bulk silver (100) were also simulated using the models with dimensions of approximately 12 nm × 12 nm × 10 nm, which contained about 129400 atoms for copper and 86400 atoms for silver. Furthermore, all indentation simulations were performed with a constant indenter tip speed of 20 m/s using a rigid spherical indenter with the radius of 4.0 nm. The kinetic energy was added into system during indentation process. The atomic force between each atom and indenter was calculated as follows:

$$F(r)=\begin{cases}-k(r-R)^2 & r>R\\ 0 & r<R\end{cases} \quad (3)$$

Where, k is the specified force constant, r is the distance from an atom to the centre of indenter, and R is the radius of an indenter.

3. Results and discussion

3.1 Misfit dislocation

The energy of system is decreased as the system approaches to the equilibrium in relaxation process. The mismatch of lattice constants in the model creates the extra atom half-planes in the copper layer with smaller lattice constant. As a result, the misfit dislocations were formed along <110> directions at the interface (001) as shown in Fig.1. In order to clearly display the misfit dislocations, a half of silver layer was removed and the dislocation atoms detected by centrosymmetry parameter method [12] were depicted in different colours depending on their magnitude of parameter. The edge misfit dislocations lay along <110> directions on boundary of extra half-plane. As the result, Burgers vector of misfit dislocations was $\frac{a}{2}[110]$ or $\frac{a}{2}[\bar{1}10]$.

3.2 Dislocation structures

Dislocation structures into models produced during indentation at zero temperature are shown in Fig. 2, where, only atoms

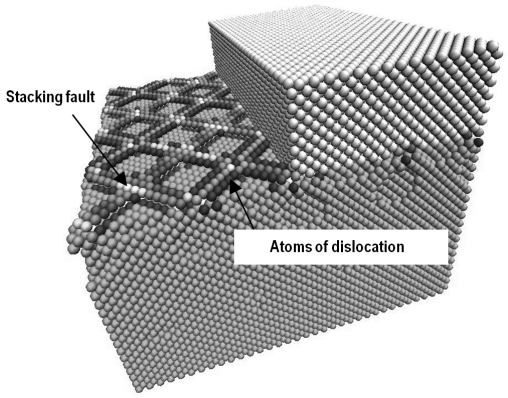

Fig. 1 The Structure of the relaxed interface.

with centrosymmetry parameter exceed 0.5 $Å^2$ were displayed. The dark colour represented the atoms of dislocation with the centrosymmetry parameter between 0.5 $Å^2$ and 5 $Å^2$, and the light colour for stacking fault with the parameter between 5 $Å^2$ and 18 $Å^2$, while atoms at bottom and top free surface with centrosymmetry parameter greater than 18 $Å^2$ were depicted as a point matrix to easily describe the dislocation structure inside model. The initial dislocations were introduced in crystalline bulk silver at indentation depth of 0.32 nm, which was about 0.75 nm underneath from the indenter. Next, the pyramidal dislocation structure was created at the place of initial dislocation. When indentation depth increased, the dislocation structure was transformed into dihedral dislocation structure, which continued gliding down and developed in size. And so on, The Shockley partial dislocation loop was dissociated from dislocation structure at indentation depth of 0.67 nm (Fig.2a). The loop quickly grew, glided and was able to separate from the main dislocation structure and continued gliding down along <011> direction until emitting at grain boundary [13]. Crystalline bulk copper is also fcc structure same as silver, dislocation growing mechanism inside bulk copper was the same as silver but process from initial dislocation to dissociation of Shockley partial dislocation loop took place from indentation depth of 0.30 nm to 6.4 nm. Certainly, this mechanism is true for Ag film/Cu substrate. Pyramidal dislocation structure in the model (Fig.2b) was formed from stacking faults (111) and Lomer-Cottrell dislocations along direction <101> and <011> on the pyramidal side edges. It was also transformed into a dihedral structure of dislocations by the deeper indentation (Fig.2c). The intersection line of the dihedral structure was dislocations lay in <110> direction. When indentation depth continues increasing, the dihedral

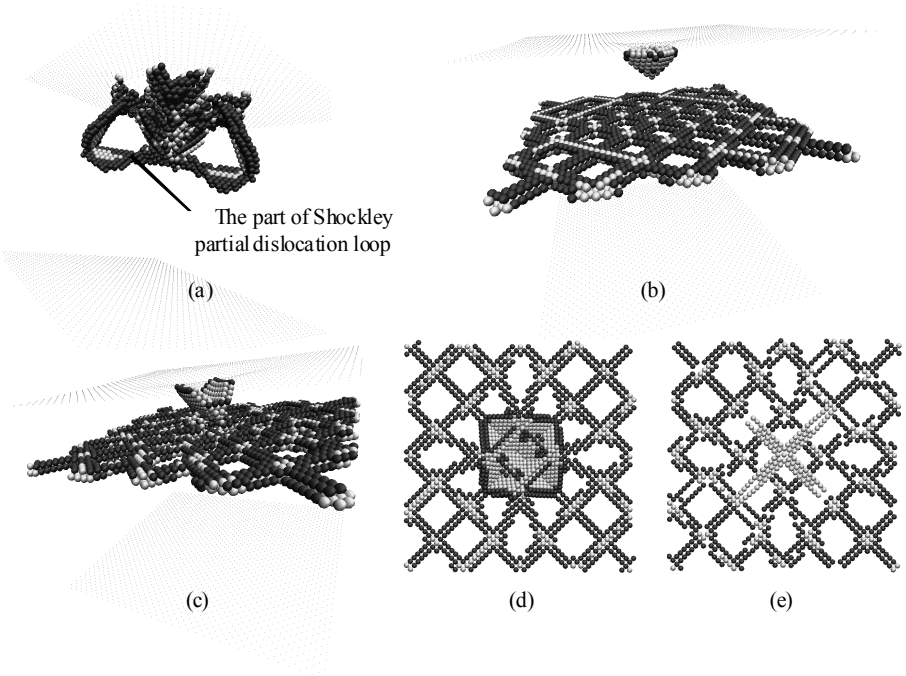

Fig. 2 Dislocation structure: (a) bulk Ag at indentation depth of 0.9 nm, (b) pyramid dislocation loop of 4.0 nm Ag film/Cu substrate at indentation depth of 0.4 nm,(c) the contact of dihedral dislocations at the interface of 3.0 nm Ag film/Cu substrate at indentation depth of 0.45 nm, (d) top view of dislocation structure of 2.0 nm Ag film/Cu substrate at indentation depth of 0.3 nm and (e) bottom view of isolated Cu atoms in dislocation of 3.0 nm Ag film/Cu substrate at indentation depth of 0.5 nm.

glided down with size increasing on the two sides along <110>direction, also supplementing stacking faults in the two planes of dihedral dislocation structure. In the case, Ag film is thin enough (less than 4.0 nm), dihedral dislocation structure would hit on the interface by dislocations in the intersection line before dissociation of Shockley partial dislocation loop, the edge misfit dislocations were dissociated and glide up to create a "flower-like" dislocation loop on the interface as shown in Fig. 2(d). On the contrary, if the Ag film is thick enough (greater than 4.0 nm), the Shockley partial dislocation loop was dissociated, quickly glided down and hit on misfit dislocation in the interface before the dihedral dislocation structure hitting on the interface. In addition, when copper atoms in misfit dislocation were isolated to study dislocation gliding as shown in Fig. 2(e), we have relied that this dislocations did not glide out of the interface.

3.3 Stiffness

The force versus indentation depth curves of crystalline copper, silver and Ag film/Cu substrate at zero temperature as well as those at room temperature are shown in Figs. 3(a) and 3(b), respectively. It is clear that the force-indentation depth curve of crystalline bulk copper is higher than that of bulk copper and copper substrate with various thickness of Ag film. The first sudden drop in force of crystalline copper and silver at indentation depth of 0.64 nm (point A) and 0.67 nm (point B) in Fig. 3 (a) were coincident to the indentation depth where part of Shockleypartial dislocation loop was dissociated from main dislocation region. The sudden drop in force in curve CuAg20 and CuAg30 (2.0 nm and 3.0 nm Ag film/Cu substrate) appeared at indentation depth of 0.27 nm (point D) and 0.54 nm (point C), respectively, earlier than bulk copper and bulk silver. Where the dihedral dislocation structure in models started hitting on the interface, misfit dislocations glided up to create a flower-like dislocation loop as mentioned above. Beyond that, the CuAg20 and CuAg30 curves decreased and clearly lower than that curve of silver. Besides, the drop in force of CuAg40 (4.0 nm Ag film/Cu substrate) and CuAg50 (5.0 nm Ag film/Cu substrate) also took place at indentation depths of 0.86 nm and 0.93 nm when the dislocations hit against the

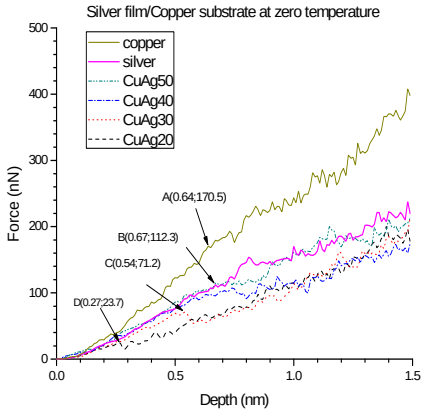

(a)

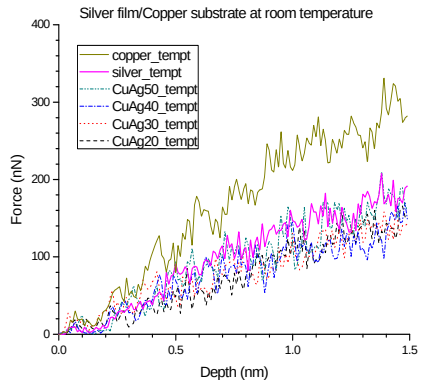

(b)

Fig. 3 Force-indentation depth curves, Cu, Ag and Ag films/Cu substrate: (a) At zero temperature, (b) at room temperature.

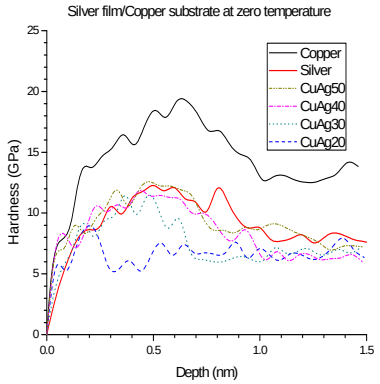

(a)

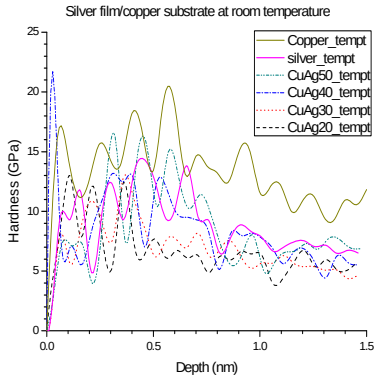

(b)

Fig. 4 Hardness-indentation depth curves, Cu, Ag and Ag films/Cu substrate: (a) At zero temperature, (b) at room temperature.

interface. Furthermore, those curves were sudden down at once Shockley partial dislocation was dissociated. Though sudden drop in force occurred in the curves by the effect of dislocation hitting and dislocation dissociation, the CuAg50 was still close to the silver curve while the CuAg40 lower than that of silver but higher than CuAg30 and CuAg20 curves. It seems that interface of multilayer materials has role as grain boundary in multi-crystal materials. Strength of multilayer materials increases with increasing in nanometres layer thickness [14] same as inverse Hall-Petch relation [15-17].

The force versus indentation depth curves of those materials at room temperature in Fig. 3(b) show that, by the thermal effect, atoms vibrated with higher magnitude and frequency. The vibration of atoms created initial dislocations inside model prior to indentation process and also effect on interaction force between indenter and atoms (Eq. 3) to make the vibration on indentation force. Thus, it is very difficult or impossible to point out the drop in force by this dislocation nucleation and also hitting of dislocation on the interface. But the trend of those curves shows that the stiffness of Ag films/Cu substrate is lower than that of bulk silver as the rule at zero temperature.

3.4 Hardness

Hardness of materials is defined by ratio of load and projected remaining contact area after unloading. It is unable to measure hardness at every time step in experimental work but in simulation. The really projected contact area would be measured each loading step instead of remaining area after

unloading based on Doerner-Nix model applied for the spherical indenter [18]. Experimental test and also simulation proved the existenceof error at region near indenter on surface by piling-up and sinking-in. Thus, all contact atoms at each time step and center of indenter were projected on a plane perpendicular to the indentation direction, in this work. This area, normally, is not circle by the error in piling-up and sinking-in as mentioned above. By the reason, average distance from projected center to the points on the area boundary was used as the radius of an equivalent circle to calculate the projected contact area. As the result, hardness versus indentation depth curves were plotted on Figs.4 (a) and (b) for Ag film/Cu substrate at zero and room temperature. It shows that the trend of the curves is similar to the force-indentation depth curves of those materials. Hardness of copper is clearly higher than that of silver as well as silver films/copper substrate. The hardness of 4.0 nm and 5.0 nm silver film/copper substrate is close to that of bulk silver while hardness curves of 2.0 nm and 3.0 nm silver film/copper substrate are clearly lower than that of bulk silver at zero temperature as shown in Fig. 4(a). The drop in hardness-indentation depth curves is the same as that in force-indentation depth curves. Hardness properties of these materials at room temperature is shown in Fig. 4(b).

Hardness of the materials at room temperature is lower than that of materials at zero temperature and its values vibrate faster but the trend of the curves is the same as that at zero temperature.

3.5 Transformation of Dislocations

Since both copper and silver are face-centred cubic (fcc) metal, the dislocations usually glide on (111) slip plane [19] and rarely glide on (001) plane. The glide of dislocation on (001) plane, normally, is not changed either characteristic or energy of dislocation. Therefore, it is less cared about. The hitting of dislocations at the interface at zero temperature (Fig. 6) is accumulated for the glide up of edge misfit dislocations with Burgers vector of $\frac{a}{2}[110]$, resulting in the dissociation into two Shockley partial dislocations and a residual dislocation as shown in Fig. 6(b). The combination of the partial dislocations bound the stacking fault at intersection of two (111) stacking faults creates the Lomer-Cottrell dislocations. In order to understand the details of dislocation reactions in the interface, a schematic diagram of dislocations with line senses for Fig. 5 (b) was presented in Fig. 5 (c). Burgers vectors of dislocations were illustrated by arrows on the dislocation line as shown in Fig. 5(d) expressing the outgoing and incoming directions of Burgers vectors at intersection points. Burgers vector would be perpendicular to the dislocation line and the stacking fault bearing that dislocation line. Conservation of Burgers vectors of the dislocation is analysed in following.

$$\text{At point } A_1: \quad \frac{a}{2}[\bar{1}10] = \frac{a}{6}[12\bar{1}] + \frac{a}{6}[\bar{2}\bar{1}1] + \frac{a}{3}[\bar{1}10] \tag{4}$$

$$\text{At point } B_1: \quad \frac{a}{2}[\bar{1}\bar{1}0] = \frac{a}{6}[1\bar{2}1] + \frac{a}{6}[\bar{2}1\bar{1}] + \frac{a}{3}[\bar{1}\bar{1}0] \tag{5}$$

$$\text{At point } C_1: \quad \frac{a}{2}[1\bar{1}0] = \frac{a}{6}[211] + \frac{a}{6}[\bar{1}\bar{2}\bar{1}] + \frac{a}{3}[1\bar{1}0] \tag{6}$$

$$\text{At point } D_1: \quad \frac{a}{2}[110] = \frac{a}{6}[\bar{1}21] + \frac{a}{6}[2\bar{1}\bar{1}] + \frac{a}{3}[110] \tag{7}$$

Each edge misfit dislocation was dissociated into two Shockley partial dislocations and residual dislocations left in the interface. These residual dislocations formed Lomer-Cottrell dislocations by meeting with stacking faults in the interface. Next, the four Lomer-Cottrell dislocations were formed at the point E_1, F_1, G_1, and H_1 when Shockley partial dislocations met at the intersection of the two stacking faults.

$$\text{At point } E_1: \quad \frac{a}{6}[12\bar{1}] + \frac{a}{6}[1\bar{2}1] = \frac{a}{3}[100] \tag{8}$$

$$\text{At point } F_1: \quad \frac{a}{6}[\bar{2}1\bar{1}] + \frac{a}{6}[211] = \frac{a}{3}[010] \tag{9}$$

$$\text{At point } G_1: \quad \frac{a}{6}[\bar{1}21] + \frac{a}{6}[\bar{1}\bar{2}\bar{1}] = \frac{a}{3}[\bar{1}00] \tag{10}$$

$$\text{At point } H_1: \quad \frac{a}{6}[2\bar{1}\bar{1}] + \frac{a}{6}[\bar{2}\bar{1}1] = \frac{a}{3}[0\bar{1}0] \tag{11}$$

The conservation of Burgers vectors were expressed through equations (4-11). Moreover, the equilibrium of all incoming Burgers vectors at point O also proved for this conservation as follow.

$$\begin{aligned} &\left\{\frac{a}{3}[110] + \frac{a}{3}[\bar{1}\bar{1}0] + \frac{a}{3}[\bar{1}10] + \frac{a}{3}[1\bar{1}0]\right\} + \\ &\left\{\frac{a}{3}[100] + \frac{a}{3}[\bar{1}00] + \frac{a}{3}[010] + \frac{a}{3}[0\bar{1}0]\right\} = 0 \end{aligned} \tag{12}$$

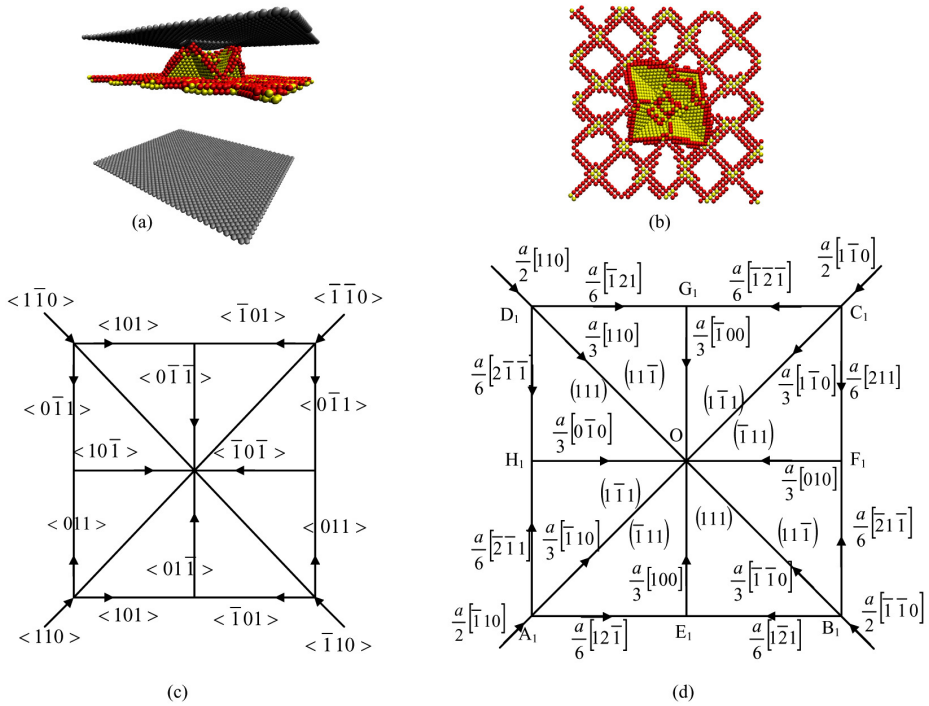

Fig. 5 Dislocation structure 3.0 nm silver film/copper substrate at indentation depth of 0.6 nm, (a) 3D view, (b) top view of the misfit dislocation in the interface, (c) Schematic of misfit dislocations with line senses, (d) Schematic of Burgers vectors.

The transformation of dislocations only happened in the two misfit dislocation line, where edge dislocation $\frac{a}{2}[\bar{1}10]$ was split into two Shockley partial dislocations $\frac{a}{6}[\bar{2}\bar{1}1]$ and a residual dislocation $\frac{a}{3}[\bar{1}10]$. The combination of partial dislocations at intersection of stacking fault created Lomer-Cottrell dislocation $\frac{a}{3}[0\bar{1}0]$. In this process, the magnitude of dislocation is changed from $a/\sqrt{2}$ into $a/\sqrt{6}$, $a\sqrt{2}/3$ and $a/3$, while the energy of a dislocation is proportional to square of themagnitude of Burgers vector. Thus, the energy of system is changed during the dislocation transformation. At the first, the square of the magnitude of edge dislocation ($\frac{a}{2}[\bar{1}10]$) of $a^2/2$ is dissociated into the two Shockley partial dislocations ($\frac{a}{6}[\bar{2}\bar{1}1]$) of $a^2/6$ and a residual dislocation ($\frac{a}{3}[\bar{1}10]$) of $2a^2/9$ (Eq. 4). Next, the energy of two Shockley partial dislocations is combined to create the Lomer-Cottrell dislocations ($\frac{a}{3}[0\bar{1}0]$) with square of the magnitude of $a^2/9$ (Eq. 8). As the result, the energy of dislocations is reduced proportionally to reduction in square of the dislocation magnitude from $a^2/2$ down to $a^2/3$.

$$\frac{a^2}{2} \rightarrow \left(\frac{a^2}{6}+\frac{a^2}{6}\right)+\frac{2}{9}a^2 \tag{13}$$

$$\left(\frac{a^2}{6}+\frac{a^2}{6}\right) \rightarrow \frac{a^2}{9} \tag{14}$$

$$\frac{a^2}{2} \rightarrow \frac{a^2}{9}+\frac{2a^2}{9}=\frac{a^2}{3} \tag{15}$$

During the transformation of dislocations, Burgers vector of the dislocations is conserved (Eqs. 4-12), but their energy is

reduced (Eq. 15). Since the elastic strain energy of system consists of energies of all dislocations, the change in dislocation energy has influenceddirectly on the mechanical behaviour. Thus the dislocation hitting in the interface and the transformation are the main reasons of drop in force and hardness of Ag film/Cu substrate.

4. Conclusions

Nanoindentation behaviour of Ag film/Cu substrate was studied by MD simulation method. It was shown that the stiffness and hardness strongly depended on the thickness of films. The stiffness and hardness increased with increasing the film thickness less than the critical value as inverse Hall-Petch relation. The stiffness and hardness of Ag film/Cu substrate are lower than those of single crystalline bulk silver. In case of Ag film/Cu substrate, the flower-like dislocation loop was created by the dislocation pile-up due to indentation on the interface when the thickness of Ag film did not exceed 4 nm. Silver atoms in misfit dislocations were dissociated and glided in <101> directions on slip planes (111) to create the flower-like structure, while the copper atoms in the misfit dislocation did not glide out of the interface. Moreover, the Burgers vector of dislocations was conserved during the dislocation transformation in the flower-like dislocation loop but dislocation energy was reduced. That might be associated with the drop in force and hardness of Ag film/Cu substrate. It may imply that the interaction between dislocations formed by indentation and misfit dislocations is a key factor for determining the mechanical properties of Ag thin film/Cu substrate.

Acknowledgements

This work has been financially supported by the Korea Research Foundation by grant No. 313-D00005. Also, this paper was majorly advised by the professor Amkee Kim of blessed memory.

References

1) Sommer J, Muschik T, C.H.R. Herzig and W. Gust, “Silver tracer diffusion in oriented Ag/Cu interphase boundaries and correlation to the boundary structure,” Acta Mater., Vol. 44, 1996, pp. 327-334.
2) Wolf U., Foiles S.M., and Fishmeiter H.F., “Study of misfit dislocation at the interface of weakly bonded metal/metal systems,” Acta Mater., Vol. 39, 1991, pp. 373-382.
3) Zhou X.W., Johnson R.A., and Wadley H.N.G., “Misfit-energy-increasing dislocation in vapour deposited CoFe/NiFe multilayers,” Phys. Rev. B, Vol. 69, 2004, 144113.
4) Labat S., Bocquet F., Gilles B., and Thomas O., “Stress and interfacial structure in Au-Ni and Ag-Cu multilayers,” Scripta Mater., Vol. 50, 2004, pp. 717-721.
5) Li Q., “Effect of dislocation source length on yield strength of nanostructured metallic multilayer thin films,” Mater. Sci. Eng. A, Vol. 493, 2008, pp. 288–291.
6) Noreyan A., Amar J.G., and Marinescu I., “Molecular dynamics simulations of nanoindentation of -SiC with diamond indenter,” Mater. Sci. Eng. B, Vol. 117, 2005, pp. 235–240.
7) Fang T.H., Wu J.H., “Molecular dynamics simulations on nanoindentation mechanisms of multilayered films.” Comput. Mater. Sci., Vol. 43, 2008, pp. 785-790.
8) Daw M.S., Baskes M.I., “Embedded-atom method: Derivation and application to impurities, surfaces, and other defects in metals,” Phys. Rev. B, Vol. 29, 1984, pp. 6443-6453.
9) Wadley H.N.G.., Zhou X.W., Johnson R.A., and Neurock M., “Mechanisms, models and methods of vapour deposition,” Prog. Mater. Sci., Vol. 46, 2001, pp. 329-377.
10) Johnson R.A., “Alloy models with theembedded atom method,” Phys. Rev. B, Vol.39, 1989, pp. 12554-12559.
11) Plimpton S.J., and Hendrickson B.A., “Parallel molecular dynamics with the embedded atom method,” edited by Mattson T. G., published by the American Chemical Society, Symposium Series 592, 1995, pp. 114-132.
12) Kelchner C., Plimpton S.J., and Hamilton J.C. “Dislocation nucleation and defect structure during surface indentation,” Phys. Rev. B, Vol. 58, 1998, pp. 11085-11088.
13) Lee Y.M., Park J.Y., Kim S.Y., Jun S.,and Im S., “Atomistic simulations of incipient plasticity under Al(111) nanoindentation,” Mech. Mater., Vol. 37, 2005, pp. 1035-1048.
14) Misra A., Hirth J.P., and Kung H., “Single-dislocation-based strengthening mechanisms in nanoscale metallic multilayers,” Philos. Mag. A, Vol. 82, 2002, pp. 2935-2951.
15) Swygenhoven H.V., Spaczer M., Caro A., and Farkas D.,

"Completing plastic deformation mechanisms in nanophase metal," Phys. Rev. B, Vol. 60, 1999, pp. 22-25.
16) Swygenhoven H.V., Derlet P.M., and Hasnaoui A., "Atomist mechanism for dislocation emission from nanosized grain boundaries," Phys. Rev. B, Vol. 66, 2002, 024101.
17) Chokshi H., Rosen A., Karch J., and Gleiter H., "On the validity of the Hall-Petch relationship in nanocrystalline materials," Scripta Metal., Vol. 23, 1989, pp.1679-1683.
18) Doerner M.F, and Nix W.D., "A method for interpreting the data from depth-sensing indentation instruments," J. Mater. Res. Vol. 1, 1986, pp. 601-609.
19) Hull A., and Bacon D.J., Introduction to Dislocations, Butterworth-Heinemann, 4th ed., 2001.